This is a copy of the published version, or version of record, available on the publisher's website. This version does not track changes, errata, or withdrawals on the publisher's site.

Anapole correlations in Sr_2IrO_4 defy the j_{eff}=1/2 model

D. D. Khalyavin and S. W. Lovesey

Published version information

Citation: DD Khalyavin and SW Lovesey. "Anapole correlations in Sr_2IrO_4 defy the j_{eff}=1/2 model." Physical Review B, vol. 100, no. 22 (2019): 224415.

DOI: 10.1103/PhysRevB.100.224415

This version is made available in accordance with publisher policies. Please cite only the published version using the reference above. This is the citation assigned by the publisher at the time of issuing the APV. Please check the publisher's website for any updates.

This item was retrieved from **ePubs**, the Open Access archive of the Science and Technology Facilities Council, UK. Please contact epubs@stfc.ac.uk or go to http://epubs.stfc.ac.uk/ for further information and policies.

Anapole correlations in Sr_2IrO_4 defy the $j_{eff} = 1/2$ model

D. D. Khalyavin[1] and S. W. Lovesey[1,2]
[1]*ISIS Facility, STFC, Didcot, Oxfordshire OX11 0QX, United Kingdom*
[2]*Diamond Light Source Ltd, Didcot, Oxfordshire OX11 0DE, United Kingdom*

(Received 8 May 2019; revised manuscript received 18 October 2019; published 17 December 2019)

Zel'dovich (spin) anapole correlations in Sr_2IrO_4 unveiled by magnetic neutron diffraction contravene the spin-orbit coupled ground state used by the $j_{eff} = 1/2$ (pseudospin) model. Specifically, spin and space know inextricable knots which bind each to the other in the iridate. The diffraction property studied in the paper is enforced by strict requirements from quantum mechanics and magnetic symmetry. It has not been exploited in the past, whereas neutron diffraction by anapole moments is established. Entanglement of the electronic degrees of freedom is captured by dyadic correlations of the anapole and position operators, and hallmarked in the diffraction amplitude by axial atomic multipoles with an even rank.

DOI: 10.1103/PhysRevB.100.224415

I. INTRODUCTION

Perovskite-type Sr_2IrO_4 possesses striking and unexpected properties that emerge from complementary interactions at an atomic level of detail. Indeed, an analogy is made between properties of Sr_2IrO_4 and the strange physics of ceramic superconductors (underdoped cuprates or high-T_c materials). To begin with, Sr_2IrO_4 is an electrical insulator whereas a vacancy in the electronic valence state suggests the contrary. The conundrum can be resolved by placing three interactions effecting iridium ions in a solid on a near-equal footing: a crystalline electric field, generated by ligands ions, a strong spin-orbit coupling, and strong electron correlations. The resulting electronic configuration can be studied with advantage using a half-integer effective (pseudospin) operator created from spin (**S**) and orbital angular momentum (**L**) [1,2]. The entanglement of **S** and **L** promotes a dependence of electronic properties on structural changes.

Spin-orbit coupling $\propto (\mathbf{S} \cdot \mathbf{L})$ is safely considered a small perturbation for most discussions of electrons in a solid. However, in heavy elements it need not be weak and $\mathbf{J} = (\mathbf{S} + \mathbf{L})$ is a good quantum number (the coupling constant increases in magnitude as Z^4 to a good approximation, where Z is the atomic number). Influence of electron correlations is enhanced, with a gap in the density of states and an insulating state for Sr_2IrO_4 [2]. An *ab initio* study of the compound does not favor a simple Slater insulator, but, instead, one created from substantial cooperation of Mott-type correlation effects [3]. A large rotation of IrO_6 octahedra about the c axis is a distinguishing feature in the compound's structure, otherwise akin to layered K_2NiF_4.

Dressed, quasiparticle, and effective operators in quantum mechanics have understandable widespread use, for they all facilitate constructs that capture many-body correlation effects and place them in tractable form. A field theory based on dressed particle operators, as opposed to the usual "bare" particle operators, no longer needs a renormalization procedure and avoids use of nonphysical quantities. In this genre, dressed states are epitomized in solutions of the Jaynes-Cummings model, where they are created by the interaction of the atom and the cavity field and serve as a paradigm of entangled (correlated) quantum systems [4–6]. In solid-state physics, quasiparticle operators appear in many formulations of electronic properties of semiconductors and metals [7]. They are also prominent in theories of conventional superconductivity through Bogolyubov transformations and formulations of the Bardeen-Cooper-Schrieffer mechanism. Effective operators for electronic degrees of freedom are the same basic concept in another guise. Operators of this type date back to the 1950s when they were introduced for electrons participating in resonance phenomena, e.g., electron paramagnetic resonance, NMR, and, later, the Mössbauer effect. A publication by Stevens in 1952, on magnetic properties of rare-earth ions, proved extremely influential at the time; since then his effective, or equivalent, operators have become a standard tool in theories of magnetic phenomena [8].

Strictures within the pseudospin model of an iridate translate to a major simplification of the amplitude for magnetic neutron diffraction that is the subject of this paper. Fortunately, steps to make the model realistic trigger radical changes to the amplitude that can be tested. A tetragonal distortion contravenes the model and allows $J = 3/2$ and $J = 5/2$ in the Ir ground state [low-spin Ir^{4+} ($5d^5$) configuration], for example. More information about this and other aspects of the ground state are gathered in an appendix. This modification alone is known to produce clear-cut changes to the diffraction amplitude [9]. An impartial approach is to test the diffraction amplitude informed by the relevant magnetic space group against measured Bragg diffraction patterns [10], and we conclude that the patterns and pseudospin-model predictions do not match. Specifically, the exact angular anisotropy is delineated, and polar (Dirac) contributions are strictly forbidden in the calculated amplitude by dint of selection rules generated from the space group.

Our method of working is far removed from that of Jeong *et al.* [10], who construct a conventional magnetization-

 ©2019 American Physical Society

density map from their diffraction patterns. They show that the map does not possess angular anisotropy predicted by the pseudospin model, and dispute between the model and diffraction patterns is common ground in the two methods of working. Jeong *et al.* [10] base their argument on a simple average of two diffraction patterns gathered with two orientations of the applied magnetic field. Our magnetic symmetry argument implies the averaging is not justified, and an informed analysis of their data that we report confirms it. Local principal Ir axes (ξ, η, ζ), with ζ labeling the field direction, are necessarily different for different directions, while Jeong *et al.* [10] recover pseudoaxes for iridium ions in an average distribution of field-induced magnetization. Beyond, we extract from measured diffraction amplitudes precisely defined atomic entities (multipoles with discrete symmetries) that can be studied in simulations of the electronic structure. In particular, we extract correlations of the electronic Zel'dovich anapole that do not exist in the pseudospin model. A third of the Bragg spots indexed by Jeong *et al.* [10] allow admixtures of axial and Dirac multipoles, while the authors assume that axial dipoles alone generate all measured Bragg spots in their analysis.

We denote an axial (parity-even) magnetic (time-odd) multipole of integer rank K by $\langle T_Q^K \rangle$, where projections Q obey $-K \leqslant Q \leqslant K$, and angular brackets $\langle \ldots \rangle$ denote the time-average, or expectation, value of the enclosed spherical operator. The dipole $\langle T_0^1 \rangle \equiv \langle T_\zeta^1 \rangle$ is a linear combination of $\langle S_\zeta \rangle$ and $\langle L_\zeta \rangle$, to a good approximation. In the forward direction of scattering $\langle \mathbf{T}^1 \rangle = \langle 2\mathbf{S} + \mathbf{L} \rangle$. This result, first given by Schwinger [11], makes neutron Bragg diffraction the method of choice for the determination of magnetic structures. [Spherical and Cartesian components of a dipole $\mathbf{R} = (x, y, z)$ are related by $x = (1/\sqrt{2})(R_{-1} - R_{+1})$, $y = (i/\sqrt{2})(R_{-1} + R_{+1})$, $z = R_0$.]

Multipoles of particular interest in our study encapsulate spin and orbital (spatial) degrees of freedom, and they are hallmarked by the fact that their rank is even [12]. In the past, they have not been included in interpretations of Bragg diffraction patterns, to the best of our knowledge. We infer values of the quadrupole ($K = 2$) in field-induced magnetization using Bragg diffraction patterns for Sr_2IrO_4 reported by Jeong *et al.* [10]. The quadrupole is proportional to the expectation value of $(R_0\Omega_0)$, where $\mathbf{R}$ and $\mathbf{\Omega} = (\mathbf{S} \times \mathbf{R})$ are dipole operators for position and the spin anapole (Dirac dipole), respectively. Evidently, the product operator $(R_0\Omega_0)$ is time odd (magnetic) and parity even as required for all axial multipoles $\mathbf{T}^K$. Specific examples of the exact proportionality between $\mathbf{T}^2$ and $(R_0\Omega_0)$ are provided in the Appendix. Hexadecapoles are proportional to expectation values of $[(R_0(7R_0^2 - 3)\Omega_0]$, and they are not included in our analysis. A quantum-mechanical selection rule forbids even-rank multipoles in a J manifold; specifically, they are forbidden in the pseudospin model with $J = 5/2$ [12].

The spin anapole $\mathbf{\Omega}$ was studied by Zel'dovich in the course of investigating parity-violating interactions in electromagnetic theory [13]. Parity violation in atomic and molecular systems with the observation of electronic anapoles can be traced back to 1974 [14–17], and anapole moments are known to diffract neutrons [18].

II. MATERIAL PROPERTIES

Sr_2IrO_4 adopts the layered K_2NiF_4 structure [10,19], and a t_{2g}-type analog of the underdoped high-T_c cuprate La_2CuO_4 [2,20,21]. Doping Sr_2IrO_4 to induce superconductivity has been investigated [22]. A square lattice of iridium ions is formed by corner-sharing IrO_6 octahedra, elongated along the c axis and rotated about it by $\approx 11^\circ$. The chemical structure is $I4_1/acd$ with Ir ions at acentric sites ($8a$) (site symmetry $\bar{4}$). The magnetic transition at a temperature ≈ 230 K results in a basal-plane antiferromagnetic order and weak ferromagnetism ascribed to a Dyzaloshinskii-Moriya interaction [21]. The magnetic motif is described by space group P_Icca that possesses an antibody-center condition and ordering wave vector (1, 1, 1) [23]. The material shows a metamagnetic transition and becomes a weak ferromagnet on application of a small magnetic field of ~ 0.2 T parallel to the plane. Interestingly, the canting moment is one to two orders of magnitude larger than that of an analogous canted antiferromagnet La_2CuO_4. The relatively large canting moment in magnetically ordered Sr_2IrO_4 is a consequence of interplay between the significant spin-orbit coupling and lattice distortion.

The low-spin state of the Ir^{4+} ($5d^5$) configuration is a single hole in a triply degenerate t_{2g} level. A Kramers doublet for the hole state uses a coherent superposition of different orbital and spin states that are linear combinations of projections from $J = 3/2$ and $J = 5/2$ manifolds. Projections obey $\Delta M = 0, \pm 4$, because of a tetrad axis of rotation symmetry, and the wave function (A1) is a component of the doublet. Descent to an insulator $j_{\rm eff} = 1/2$ model with $J = 5/2$ occurs through strong correlations (a large Hubbard $U \sim 2$ eV opens a gap [3]) and neglect of a tetragonal perturbation. The Kramers doublet for an octahedral crystal-field potential is a singular state, in the sense that all remaining states of the d^5 configuration are admixtures of $J = 3/2$ and $J = 5/2$ manifolds whereas the doublet is pure $J = 5/2$. Applications of the $j_{\rm eff} = 1/2$ (pseudospin) model [2,20] are mainly to perovskite and honeycomb-type iridium oxides (iridates), topological phases, magnetic heterostructures, and Kitaev magnetism [21,24]. The simplicity of the model is a major attraction, and it mirrors its exclusive use of the Kramers doublet and total angular momentum $J = 5/2$.

Neutron-diffraction experiments of interest utilized a sample environment with a temperature = 4 K and an applied magnetic field, $\mathbf{H}$, with strength up to 5 T (a 5-T magnetic field corresponds to an energy ~ 0.30 meV while the iridium spin-orbit parameter ~ 380 meV) [10]. The resultant field-induced magnetization is described by orthorhombic space groups. Two field directions were employed in the experiments: (I) $Ib'c'a$ (73.551) with Ir ion in sites $8c$ for $\mathbf{H} \parallel [0, 1, 0]$, and (II) $Fd'd'd$ (70.530) using sites $16f$ for $\mathbf{H} \parallel [-1, 1, 0]$ [23]. Iridium site symmetry is acentric in both magnetic space groups. The weakly ferromagnetic state induced by the field keeps the large spin canting inherited from a zero-field scenario, resulting in the big net moment $\sim 0.08\,\mu_B$/Ir [10]. This implies swapping the antiferromagnetic dipole component as shown in Fig. 1 (to preserve the antisymmetric exchange) and corresponding change of the magnetic ordering wave vector from (1, 1, 1) to (0, 0, 0). Two sets of local Ir coordinates (ξ, η, ζ) are necessary; $\boldsymbol{\xi} \propto [0, 0, c]$, $\boldsymbol{\eta} \propto [a, 0, 0]$, $\boldsymbol{\zeta} \propto [0, a, 0]$ for (I),

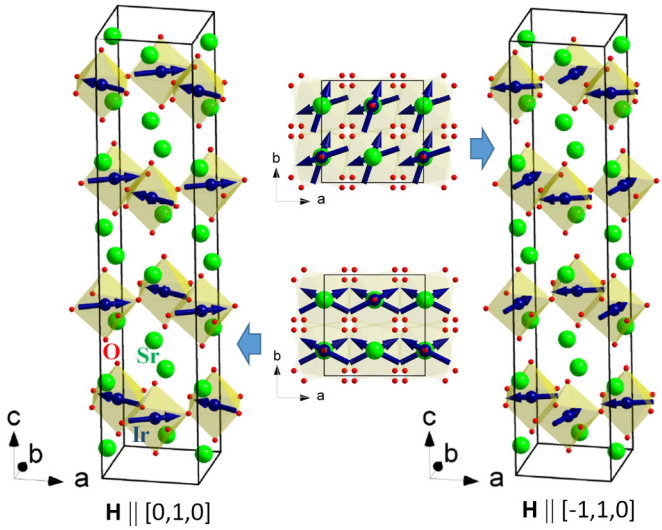

FIG. 1. Top panel: Field-induced magnetic structures for the cases (I) and (II) when the magnetic field is applied along [0,1,0] (left) and [−1,1,0] (right), respectively. The corresponding magnetic space groups are (I) $Ib'c'a$ and (II) $Fd'd'd$. Cell lengths $a = b \approx 5.484$ Å and $c \approx 25.804$ Å at 13 K [11].

and $\boldsymbol{\xi} \propto [a, a, 0]$, $\boldsymbol{\eta} \propto [0, 0, c]$, $\boldsymbol{\zeta} \propto [a, -a, 0]$ for (II). Note that the $\boldsymbol{\zeta}$ axis coincides with the magnetization direction. Motifs of allowed quadrupole moments are depicted in Fig. 4, and they have $(\xi\eta)$-type spatial symmetry. A unit vector for the direction of the Bragg wave vector $\boldsymbol{\kappa} = (\kappa_\xi, \kappa_\eta, \kappa_\zeta)$. Integer Miller indices (H_o, K_o, L_o) for the tetragonal parent structure satisfy $(H_o + K_o + L_o)$ even.

III. DIFFRACTION AMPLITUDE

A magnetic amplitude for Bragg diffraction can be obtained from an electronic structure factor, Ψ^K_Q, that obeys all symmetry in a magnetic space group. To this end, Ψ^K_Q is a sum over sites at positions $\mathbf{d}$ in a unit cell occupied by iridium ions, to which we assign a magnetic multipole $\langle \mathcal{O}^K_Q \rangle$ defined to have discrete symmetry with respect to inversion of spatial coordinates. Sites in a cell are related by symmetry operations that are translations plus twofold rotations and inversions. Time reversal does not occur in the construction of Ψ^K_Q, but it is present in iridium site symmetry that is $2'_\xi$ and $2'_\eta$ for cases (I) and (II), respectively. A phase factor $\exp(i\boldsymbol{\kappa}\cdot\mathbf{d})$ accompanies each multipole in Ψ^K_Q. With Miller index $L_o = 4n$, we find

$$\Psi^K{}_Q(\mathrm{I}) = 2\exp(i\varphi_\mathrm{I})\langle \mathcal{O}^K{}_Q\rangle_\mathrm{I}[1 + (-1)^Q\sigma_\pi][1 + (-1)^{K_o}\sigma_\pi], \tag{1}$$

$$\Psi^K{}_Q(\mathrm{II}) = 4\exp(i\varphi_\mathrm{II})\langle \mathcal{O}^K{}_Q\rangle_\mathrm{II}[1 + (-1)^Q][1 + (-1)^{H_o}\sigma_\pi]. \tag{2}$$

Spatial phases are $\varphi_\mathrm{I} = \{\pi(n + K_o/2)\}$ and $\varphi_\mathrm{II} = \{\pi(-n + H_o/2)\}$, and the parity signature $\sigma_\pi = +1(-1)$ for axial (Dirac) varieties of $\langle \mathcal{O}^K_Q \rangle$. Bulk properties are presented by (1) and (2) evaluated for $H_o = K_o = L_o = 0$, and evidently both structure factors can be different from zero for axial multipoles $\langle T^K_Q \rangle$. Moreover, in (1) and (2) projections $|Q|$ are restricted to even integers, which means $Q = 0$ for dipoles $(K = 1)$, i.e., bulk axial magnetism $\propto \langle T^1{}_0 \rangle$ is allowed in the direction of the applied magnetic field, as expected. In Bragg diffraction patterns of interest, H_o and K_o are even. In consequence, Dirac multipoles with $\sigma_\pi = -1$ are absent from the electronic structure factors. Hereafter, $\sigma_\pi = +1$, with corresponding axial multipoles $\langle T^K_Q \rangle$, and $|Q|$ are even integers. In addition, site symmetry requires $\langle T^K_Q \rangle = -(-1)^K \langle T^K_{-Q} \rangle$. We quote an amplitude per magnetic ion derived from (1) and (2) and divided by 8 and 16, respectively.

Multipoles and components of the unit Bragg wave vector, $\boldsymbol{\kappa}$, are specific to the induced magnetization defined by magnetic space groups (I) $Ib'c'a$ and (II) $Fd'd'd$ [11]. (I) $\kappa_\xi = \aleph(aL_o/c)$, $\kappa_\eta = \aleph H_o$, $\kappa_\zeta = \aleph K_o$, with $\aleph = [H_o^2 + K_o^2 + (aL_o/c)^2]^{-1/2}$. The magnetic amplitude $F_M(\boldsymbol{\kappa})$ is a function of $(\kappa_\alpha)^2$ and it does not depend on the signs of Miller indices H_o and K_o, in the present case. However, $F_M(\boldsymbol{\kappa})$ is not symmetric in the two indices. (II) $\kappa_\xi = \aleph(H_o + K_o)/\sqrt{2}$, $\kappa_\eta = \aleph(aL_o/c)$, $\kappa_\zeta = (H_o - K_o)/\sqrt{2}$. The corresponding $F_M(\boldsymbol{\kappa})$ is the same for (H_o, K_o, L_o) and (K_o, H_o, L_o). However, the signs of H_o and K_o do matter, in this case. The magnitude of the Bragg wave vector $\kappa = (2\pi)/(a\aleph)$. The structure factor for iridium nuclei F_N with $L_o = 4n$ is independent of n. Moreover, $|F_N(H_o, K_o, 4n)| = |F_N(K_o, H_o, 4n)|$ and signs of H_o and K_o are irrelevant.

$F_M(\boldsymbol{\kappa})$ is the component of the magnetic scattering amplitude in the direction of the field-induced magnetization [10]. We include in $F_M(\boldsymbol{\kappa})$ symmetry-allowed dipoles $(K = 1)$, quadrupoles $(K = 2)$, and octupoles $(K = 3)$. According to the magnetic space groups multipoles possess projections $Q = 0$ ($\boldsymbol{\zeta}$ axis) and ± 2. The generic result for an abbreviated amplitude informed by magnetic symmetry is purely real [12],

$$\begin{aligned} F_M(\boldsymbol{\kappa}) \approx {} & \left\{\langle(2\mathbf{S} + \mathbf{L})_\zeta\rangle\langle j_0(\kappa)\rangle + \left(5\kappa_\zeta^2 - 1\right)\langle T^3{}_0\rangle\right\} \\ & + \left[\left(\kappa_\xi^2 - \kappa_\eta^2\right)/\left(1 - \kappa_\zeta^2\right)\right]\left\{\langle T^2{}_{+2}\rangle'' \right. \\ & \left. + \left(1 - 3\kappa_\zeta^2\right)\langle T^3{}_{+2}\rangle'\right\}. \end{aligned} \tag{3}$$

Diffraction patterns are most often analyzed with the simple approximation $F_M \approx [\langle(2\mathbf{S} + \mathbf{L})_\zeta\rangle\langle j_0(\kappa)\rangle]$, where $\kappa = (4\pi)\sin(\theta)/\lambda$ is the magnitude of the Bragg wave vector and $\langle j_0(\kappa)\rangle$ a standard radial integral [10,12]. The property $\langle j_0(0)\rangle = 1$ leaves the simple $F_M(0)$ equal to the magnetic moment $\langle(2\mathbf{S} + \mathbf{L})_\zeta\rangle$ [11]. Orbital angular momentum, which appears in the so-called dipole approximation, is omitted from (3) since it does not influence angular anisotropy (the Appendix contains additional information). Termination of the amplitude (3) at the level of octupoles is usually justified on the grounds that multipoles with ranks $K \geqslant 4$ are very small in the range of wavevectors of interest, and we find this to be an entirely reasonable approximation to the data in hand. The quadrupole $\langle T^2{}_{+2}\rangle''$ is proportional to $\langle j_2(\kappa)\rangle$. Octupoles are linear combinations of $\langle j_2(\kappa)\rangle$ and $\langle j_4(\kappa)\rangle$, and some relevant examples are in the Appendix. We use $'$ and $''$ to denote real and imaginary parts of multipoles, while a multipole with projection $Q = 0$ is purely real. With $\langle j_n(0)\rangle = 0$ for $n \geqslant 2$ the amplitude (3) obeys $F_M(0) = \langle(2\mathbf{S} + \mathbf{L})_\zeta\rangle$, and the reported value of the induced moment =0.08 [10]. By way

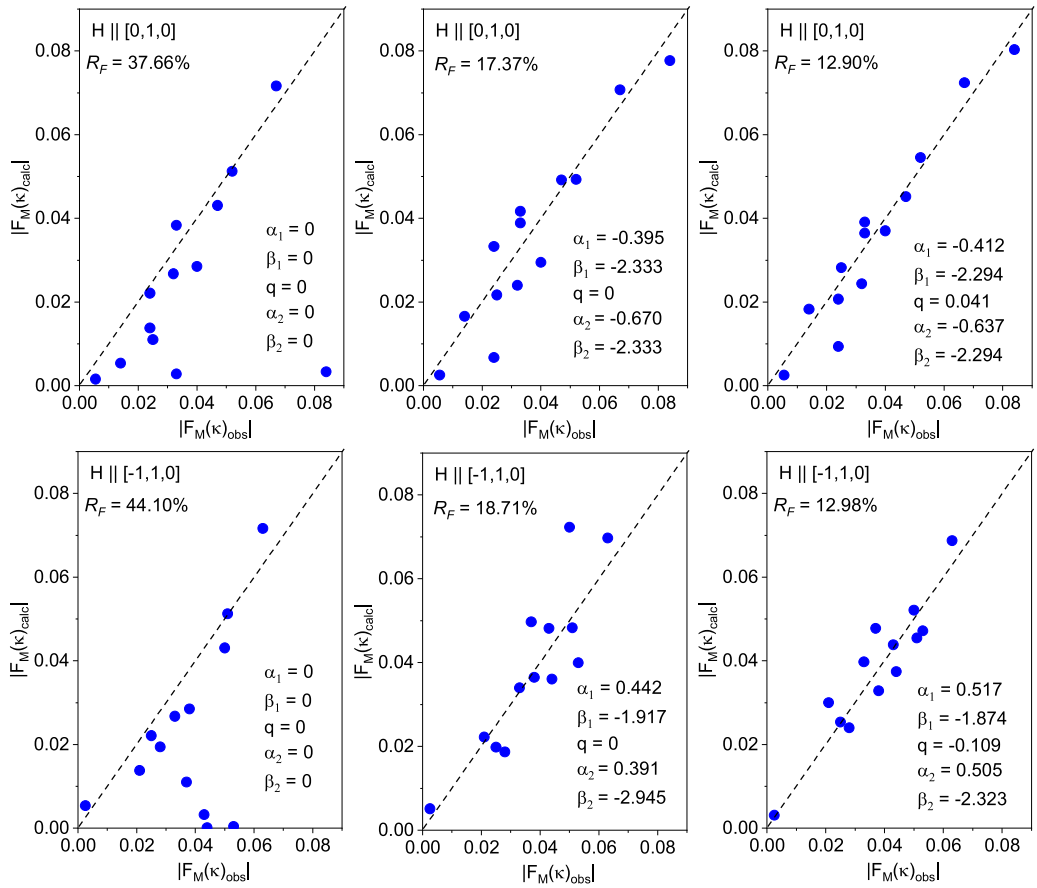

FIG. 2. Fits to data for the two magnetic -field directions labeled (I) (13 Bragg spots, top row) and (II) (13 Bragg spots, bottom row) in the main text. Sample temperature 4 K and field strength up to 5 T. Parameters determine multipoles $\langle T^2{}_{+2}\rangle'' = [q\langle j_2(\kappa)\rangle]$, $\langle T^3{}_0\rangle = \{\alpha_1[\langle j_2(\kappa)\rangle + \beta_1\langle j_4(\kappa)\rangle]\}$, and $\langle T^3{}_{+2}\rangle' = \{\alpha_2[\langle j_2(\kappa)\rangle + \beta_2\langle j_4(\kappa)\rangle]\}$. From left to right, fit to $F_M \approx [\langle(2\mathbf{S}+\mathbf{L})_\zeta\rangle\langle j_0(\kappa)\rangle]$ with $\langle(2\mathbf{S}+\mathbf{L})_\zeta\rangle = 0.08$, fit to (3) with $q = 0$, and, finally, fit with all three multipoles. Bragg diffraction data reported by Jeong *et al.* [10] include 38 spots of which 26 used here obey selection rules $L_o = 4n$ included in our magnetic amplitude (3).

of background information, the quadrupole $\langle\mathbf{T}^2\rangle$ and octupole $\langle\mathbf{T}^3\rangle$ supported by the antiferromagnetic motif (zero applied field) are discussed in the Appendix.

IV. DATA AND THEORY

We confront the magnetic amplitude (3) with experimental data for field-induced amplitudes in Sr_2IrO_4 at a temperature = 4 K [10]. To begin with, the simple approximation $F_M \approx [\langle(2\mathbf{S}+\mathbf{L})_\zeta\rangle\langle j_0(\kappa)\rangle]$ displayed in Fig. 2 returns goodness-of-fits $R_F = 37.66\%$ and $R_F = 44.10\%$ for field directions labeled (I) and (II), respectively. Angular anisotropy in $F_M(\boldsymbol{\kappa})$ is reported to be extremely large in the high-κ reflections, e.g., (4, 2, 0) and (2, 0, 20) with $\sin(\theta)/\lambda \approx 0.41$ Å^{-1} and 0.43 Å^{-1}, respectively [10]. Moving ahead, we use the exact representation $\langle T^2{}_{+2}\rangle'' = [q\langle j_2(\kappa)\rangle]$, and infer a value of the quadrupole parameter q from data. By way of orientation to a significant fit to data we first experimented with a parametrization $\langle T^3{}_0\rangle = [pt(\kappa)]$ and $\langle T^3{}_{+2}\rangle' = [rt(\kappa)]$ that is correct within a J manifold used by the pseudospin model. Tolerable agreement was found with $(q/p) \approx -0.3$, $r \approx -0.1$ and $(q/p) \approx -0.5$, $r \approx -2.0$ for cases (I) and (II), respectively. The common dependence on the wave vector, $t(\kappa)$, inferred from fits to Bragg diffraction patterns was very different for the two cases, however, and the restriction was abandoned in more extensive analyses.

To investigate the indication of a difference between field directions more fully, and consolidate results for q, we used exact representations $\langle T^3{}_Q\rangle' = \{\alpha_f[\langle j_2(\kappa)\rangle + \beta_f\langle j_4(\kappa)\rangle]\}$ with $f = 1$ and 2 for $Q = 0$ and $Q = +2$, respectively. As already mentioned, for a J manifold the wave-vector dependence of multipoles is fixed by their rank, i.e., $\beta_1 = \beta_2$ for the two octupoles of interest, and $\beta_1 = (2/9)$ reported in the Appendix is correct for $J = 5/2$ [12]. After the said parametrization of quadrupoles, $F_M(\boldsymbol{\kappa})$ contains five parameters to be inferred from data. Radial integrals in the fits to data are appropriate for isolated Ir^{4+} (Kobayashi *et al.* [25]) with no attempt on our part to simulate departures due to solid-state effects.

The good fits of $F_M(\boldsymbol{\kappa})$ to 26 measurements displayed in Fig. 2 vindicate its intrinsic merit; $R_F = 12.90\%$ (17.37%) and $R_F = 12.98\%$ (18.71%) for field directions labeled (I) and (II), respectively, and values achieved with $q = 0$ are in brackets. It is beyond reasonable doubt that the quadrupole $\langle T^2{}_{+2}\rangle'' = [q\langle j_2(\kappa)\rangle]$ is significant for both field directions. A useful measure of its physical importance is the relative roles of $\langle T^2{}_{+2}\rangle''$ and the diagonal octupole $\langle T^3{}_0\rangle$ in fits to data, and inferred ratios $q/\alpha_1 \approx -0.10$ and -0.21 for (I) and

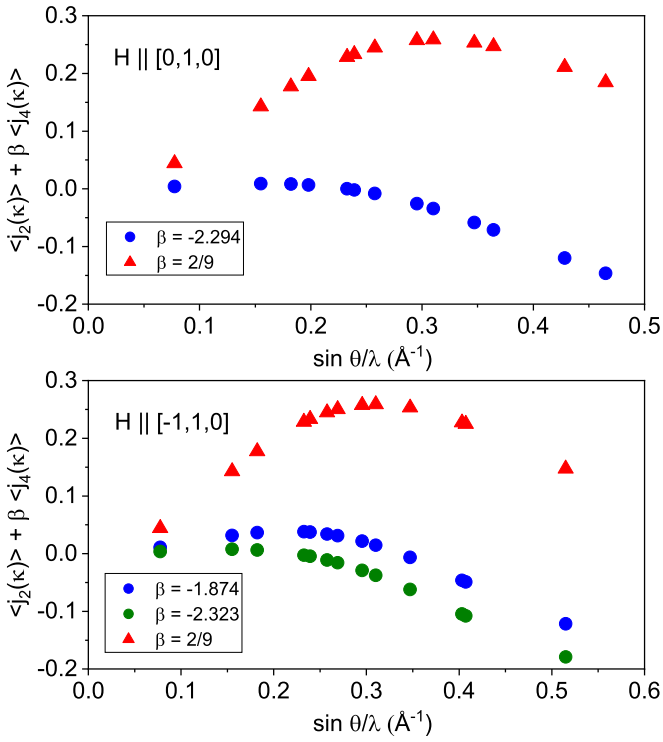

FIG. 3. $[\langle j_2(\kappa)\rangle + \beta\langle j_4(\kappa)\rangle]$ for various β as a function of $\kappa/(4\pi) = \sin(\theta)/\lambda(\text{Å}^{-1})$ determined by measured Bragg spots, as in Fig. 2. Red triangles $\beta = (2/9)$ appropriate for the $J = 5/2$ manifold used by the pseudospin model [8,12]. Top panel field direction labeled (I); blue spots $\beta = -2.294$ inferred from data. Bottom panel case (II); blue (green) spots $\beta = -1.874$ (-2.323). Radial integrals $\langle j_n(\kappa)\rangle$ for Ir^{4+} taken from Ref. [20] and $\langle j_2(0)\rangle = \langle j_4(0)\rangle = 0$.

(II) are similar to those retrieved by experimenting with fits to diffraction patterns using a common dependence $t(\kappa)$. Such is the case for field direction (I) where we find $\beta_1 \approx \beta_2 \approx -2.294$. On the other hand, $\beta_2/\beta_1 \approx 1.24$ for field direction (II). Inferred values of β_f bracket ≈ -1.9 and ≈ -2.3 and emphatically rule against use of the $J = 5/2$ manifold. Regarding the signs of inferred parameters for the two octupoles, $\langle T^3{}_0\rangle$ and $\langle T^3{}_{+2}\rangle'$, note that β_f is of one sign for both (I) and (II), while α_f is of one sign within each ferromagnetic state. We have no firm insight as to why signs of βs are different for antiferromagnetic [$\beta = +1.005$ in Eq. (A4)] and field-induced motifs (β_f), nor why the sign of inferred α_f is different for (I) and (II). However, a switch in sign of q and α_f between (I) and (II), namely, $\pm q$ and $\mp\alpha_f$, suggests a correlation with the ferromagnetic motif.

Figure 3 displays the radial dependence $[\langle j_2(\kappa)\rangle + \beta_f\langle j_4(\kappa)\rangle]$ of octupoles $\langle T^3{}_0\rangle$ and $\langle T^3{}_{+2}\rangle'$ using β_f inferred from diffraction patterns for field directions (I) and (II). As reference values, we include $[\langle j_2(\kappa)\rangle + (2/9)\langle j_4(\kappa)\rangle]$ for the pseudospin model. We have established two motifs of quadrupoles $\langle T^2{}_{+2}\rangle''$ with $(\xi\eta)$-type spatial symmetry depicted in Fig. 4. It is worth noting that a logical improvement to (3) admits two hexadecapoles, $\langle T^4{}_{+2}\rangle''$ and $\langle T^4{}_{+4}\rangle''$ proportional to $\langle j_4(\kappa)\rangle$ [9,12], that will increase the number of parameters to seven ($\langle T^4{}_0\rangle$ is forbidden by site symmetry).

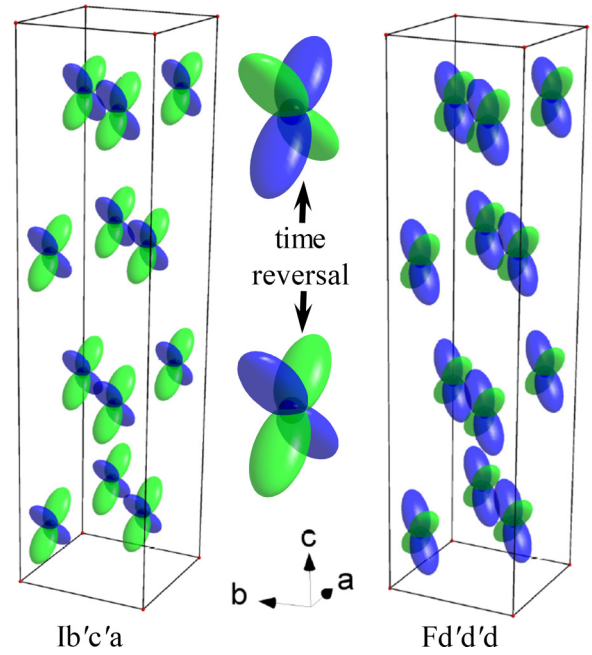

FIG. 4. Depiction of quadrupole moments $\langle T^2{}_{+2}\rangle''$.

V. CONCLUSIONS AND DISCUSSION

In summary, we have exposed dyadic correlations of anapole and position operators in Sr_2IrO_4 that do not exist in the $j_{\text{eff}} = 1/2$ (pseudospin) model of the spin-orbit coupled ground state. (Anapoles—-Dirac dipoles—-are known to be essential entities in the science of a raft of materials, including magnetoelectrics and high-T_c superconducting materials [26–28].) Empirical evidence for the correlations is derived from neutron Bragg diffraction patterns [10]. Correlation functions in question have not been exposed in previous investigations of magnetic materials, to the best of our knowledge. They are spherical atomic multipoles with an even rank defined to possess axial and magnetic discrete symmetries. Principal axes (ξ, η, ζ) for Ir ions are specific to the direction of the applied magnetic field, which is parallel to the ζ axis. In the present case, allowed quadrupoles displayed in Fig. 4 have spatial symmetry $\propto (\xi\eta)$. Quantum-mechanical selection rules in atomic physics forbid even rank multipoles in a J manifold used by the pseudospin model. Magnetic space groups, for two field directions used in the experiments [10], that we derive allow axial multipoles in diffraction patterns chosen for investigation, and the exact angular anisotropy of a pattern is delineated. Interestingly, Dirac multipoles are forbidden in diffraction under specific conditions although they are allowed by Ir site symmetry. It would be difficult to infer good values for axial multipoles from diffraction patterns that are admixtures of contributions from axial and Dirac multipoles.

Atomic properties of an iridium ion in antiferromagnetically ordered Sr_2IrO_4 are reviewed in an appendix. The t_{2g} manifold in the presence of a tetragonal crystal potential, with axial distortion along the c axis, and spin-orbit coupling, is consistent with an iridium ground-state wave function constructed from two J manifolds [1]. The axial distortion is absent in the $j_{\text{eff}} = 1/2$ (pseudospin) model. In consequence,

the model is an exclusive property of a manifold ($J = 5/2$) not populated by atomic multipoles with an even rank. The latter are signatures of J mixing, beyond the pseudospin model, and compulsory members of a realistic model of an iridate where spin and space know inextricable knots which bind each to the other. Parity-even multipoles with even rank in neutron scattering are correlations of space and anapole variables [12].

Use of magnetic multipoles to encapsulate electronic degrees of freedom affords a means by which to move the knowledge of iridates forward by other techniques [27]. Already, multipoles can be estimated with a program that is available for the interpretation of x-ray absorption and scattering experiments [29], while a different computational method has been exploited to estimate an exotic ordering of odd-rank multipoles in URu_2Si_2 [30].

ACKNOWLEDGMENTS

We thank P. Bourges for a preprint of Ref. [10], additional datasets, and valuable comments. S.W.L. is grateful to P. Bargueño, L. C. Chapon, E. W. L. Grindrod, Sir Peter Knight, and Svetlana Kozlova for assistance and guidance.

APPENDIX

By way of an introduction to multipoles in magnetic neutron diffraction, we explore multipoles supported by a minimal model of spontaneous antiferromagnetic order in Sr_2IrO_4, with a saturation moment $\mu_o \approx 0.21\,\mu_B$ in accord with a measurement [31,32]. Results serve as an orientation to the analysis of diffraction patterns for field-induced ferromagnetism in Secs. III and IV. However, there are important caveats for attempts at direct comparisons. Spatial symmetries of the minimal model and field-induced magnetizations are totally different, of course. Specifically, projections Q of spherical, parity-even ($\sigma_\pi = +1$) multipoles, $\langle T_Q^K \rangle$, are even integers (odd integers) for a field-induced (antiferromagnetic) motif. Also, magnetic moments set a scale for numerical values of multipoles and these differ by a factor $\approx$0.08/0.21. Applied to resonant x-ray Bragg diffraction, our model produces zero intensity at the L_2 absorption edge, in accord with measurements [33]. Magnetic dipole moments are confined to the a-b plane, whereas Kim *et al.* invoke dipoles parallel to the c axis in their erroneous interpretation of diffraction data gathered at the L_3 edge [31,33].

Results for neutron diffraction by a saturated ion are worth noting as a prelude. Atomic states $|J, M\rangle$ have a projection $M = J$ in the saturated configuration. The parity-even dipole $\langle \mathbf{T}^1 \rangle$ has one component parallel to the axis of quantization, labeled by projection $Q = 0$ (ζ axis of our local coordinates). In the forward direction of scattering (trivial Bragg spot $\boldsymbol{\kappa} = 0$), $\langle J, J|T^1{}_0|J, J\rangle = (g_o J) = (2S + L) = 3$, using $J = 5/2$, $L = 2$, $S = 1/2$ to obtain $g_o = (6/5)$ for the Landé factor (multipoles differ by a factor 3 from a previous definition [9,12]). Even-rank multipoles are zero in the absence of J mixing. The diagonal component of the octupole $\langle J, J|T^3{}_0|J, J\rangle = \{(18/7)(1/\sqrt{7})[\langle j_2(\kappa)\rangle + (2/9)\langle j_4(\kappa)\rangle]\}$, which vanishes in the forward direction of scattering.

Quadrupoles have no matrix elements diagonal in J. For J values of immediate interest one finds $\langle 5/2, 3/2|T^2{}_0|3/2, 3/2\rangle = -\{(15/\sqrt{2})\langle j_2(\kappa)\rangle\langle 5/2, 3/2|(R_0\,\Omega_0)|3/2, 3/2\rangle\}$, where $\mathbf{R}$ and $\boldsymbol{\Omega} = (\mathbf{S} \times \mathbf{R})$ are dipole operators for position and the spin anapole, respectively [12]. In addition, $\langle 5/2, 5/2|T^2{}_{+2}|3/2, 1/2\rangle = \{[\sqrt{5}/(2\sqrt{3})]\langle 5/2, 3/2|T^2{}_0|3/2, 3/2\rangle\} = -i\{(5/14)\sqrt{(15/2)}\langle j_2(\kappa)\rangle\}$ will arise in a simulation of field-induced magnetization. Note that matrix elements of $\mathbf{T}^2$ are purely imaginary, and the numerical coefficient in $\langle 5/2, 5/2|T^2{}_{+2}|3/2, 1/2\rangle$ is almost the same as the numerical coefficient in the foregoing $\langle J, J|T^3{}_0|J, J\rangle$ with $J = 5/2$.

Turning to an Ir ion in antiferromagnetically ordered Sr_2IrO_4, the t_{2g} manifold in the presence of a tetragonal crystal potential, with axial distortion along the c axis, and spin-orbit coupling, is consistent with an iridium ground-state wave function constructed from [1]

$$|u\rangle = \alpha|3/2, -3/2\rangle + \beta|5/2, -3/2\rangle + \gamma|5/2, 5/2\rangle. \quad \text{(A1)}$$

The selection rule $\Delta M = 0, \pm 4$ in (A1) is imposed by the tetrad axis of rotation symmetry, which is absent in the field-induced motifs $Ib'c'a$ (No. 73.551) and $Fd'd'd$ (No. 70.530). Real coefficients satisfy $(\alpha^2 + \beta^2 + \gamma^2) = 1$, and $\alpha = 0$ in the absence of a distortion. The magnetic ground-state wave function can be modeled by a linear combination of $|u\rangle$ and the conjugate state of the Kramers doublet $|\bar{u}\rangle$ [31]. A state $[|u\rangle + \Re|\bar{u}\rangle]$ with $|\Re|^2 = 1$ does not possess a magnetic dipole parallel to the c axis, and $\mu_o = \sqrt{[(\mu_a)^2 + (\mu_b)^2]} = 0.207\,\mu_B$ for $\alpha = 0.763$, $\beta = -0.409$, $\gamma = -0.500$. For simplicity, let the magnetic moment be confined to the crystal a axis. Local Ir axes ($\boldsymbol{\xi}$, $\boldsymbol{\eta}$, $\boldsymbol{\zeta}$) are $\xi \propto [0,\ 0,\ -c]$, $\boldsymbol{\eta} \propto [0,\ a,\ 0]$, $\boldsymbol{\zeta} \propto [a,\ 0,\ 0]$. The dipole $\langle \mathbf{T}^1 \rangle$ has one component,

$$\langle T^1{}_\zeta \rangle = 0.549\{[\langle j_0(\kappa)\rangle + (4/7)\langle j_2(\kappa)\rangle] + \chi[\langle j_0(\kappa)\rangle - (1/2)\langle j_2(\kappa)\rangle]\}, \quad \text{(A2)}$$

with $\chi = (\alpha/3\beta) = -0.623$ a measure of the mixing of atomic states $J = 3/2$ and $J = 5/2$. The result (A2) merits comment. In the forward direction of scattering, radial integrals take values $\langle j_0(0)\rangle = 1$ and $\langle j_2(0)\rangle = 0$ that yield $\langle T^1{}_\zeta \rangle = \mu_o$, as required [11]. Furthermore, in the contribution from the $J = 5/2$ state ($\chi = 0$), used by the $j_{\rm eff} = 1/2$ model, the exact coefficient of $\langle j_2(\kappa)\rangle$ is (4/7) and not $\{\langle \mathbf{L}_\zeta \rangle / \langle (2\mathbf{S} + \mathbf{L})_\zeta \rangle\} = 2/3$ in the so-called dipole approximation for $\langle \mathbf{T}^1 \rangle$ [12]. The approximation does account for J mixing, the hallmarks of which are even-rank multipoles. In the minimal model, the quadrupole has $(\xi\eta)$-type spatial symmetry, and

$$\langle T^2{}_{+1} \rangle'' = -0.528\langle j_2(\kappa)\rangle. \quad \text{(A3)}$$

The octupole $\langle T^3{}_{+1} \rangle'$ has $[\xi(5\eta^2 - 1)]$-type spatial symmetry, and

$$\langle T^3{}_{+1} \rangle' = -0.051\{6[\langle j_2(\kappa)\rangle + (2/9)\langle j_4(\kappa)\rangle] + \chi[\langle j_2(\kappa)\rangle - (3/4)\langle j_4(\kappa)\rangle]\}. \quad \text{(A4)}$$

With $\chi = -0.623$, there is significant departure of the κ dependence of the octupole from that with a saturated ion.

[1] A. Abragam and B. Bleaney, in *Electron Paramagnetic Resonance of Transition Ions* (Clarendon, Oxford, 1970), Sec. 7.8.

[2] B. J. Kim, H. Jin, S. J. Moon, J.-Y. Kim, B.-G. Park, C. S. Leem, J. Yu, T. W. Noh, C. Kim, S.-J. Oh, J.-H. Park, V. Durairaj, G. Cao, and E. Rotenberg, Phys. Rev. Lett. **101**, 076402 (2008).

[3] R. Arita, J. Kuneš, A. V. Kozhevnikov, A. G. Eguiluz, and M. Imada, Phys. Rev. Lett. **108**, 086403 (2012).

[4] E. T. Jaynes and F. W. Cummings, Proc. IEEE **51**, 89 (1963).

[5] B. W. Shore and P. L. Knight, J. Mod. Optics **40**, 1195 (1993).

[6] The Jaynes-Cummings model (JCM) [4] exploits a neoclassical radiation theory in which the source is quantized but the radiation field is not. The journey to a fully quantized JCM based on QED field theory stimulated important quantum-optics advances [5]. Sir Rudolf Peierls opined that the Jaynes-Cummings paper was the most influential incorrect paper in physics; S. Stenholm, J. Phys. B **46**, 224013 (2013).

[7] W. G. Aulbur, L. Jönsson, and J. W. Wilkins, in *Solid State Physics*, edited by H. Ehrenreich and F. Spaepen (Elsevier, New York, 2000), Vol. 54, p. 1.

[8] K. W. H. Stevens, Proc. Phys. Soc. A **65**, 209 (1952).

[9] S. W. Lovesey and D. D. Khalyavin, J. Phys.: Condens. Matter **26**, 322201 (2014).

[10] J. Jeong, B. Lenz, A. Gukasov, X. Fabreges, A. Sazonov, V. Hutanu, A. Louat, C. Martins, S. Biermann, V. Brouet, Y. Sidis, and P. Bourges, arXiv:1904.09139 (2019).

[11] J. S. Schwinger, Phys. Rev. **51**, 544 (1937).

[12] S. W. Lovesey, Phys. Scr. **90**, 108011 (2015).

[13] Y. B. Zel'dovich, J. Exp. Theor. Phys. **6**, 1184 (1958).

[14] M. A. Bouchiat and C. Bouchiat, J. Phys. France **35**, 899 (1974).

[15] V. L. Flambaum and I. B. Khriplovich, On the enhancement of parity non-conserving effects in diatomic molecules, preprint INP 84-167 (Novosibirsk, Russia, 1984).

[16] I. B. Khriplovich, *Parity Non-conservation in Atomic Phenomena* (Gordon and Breach, Philadelphia, 1991).

[17] A. Dorta-Urra and P. Bargueño, Symmetry **11**, 661 (2019).

[18] S. W. Lovesey, T. Chatterji, A. Stunault, D. D. Khalyavin, and G. van der Laan, Phys. Rev. Lett. **122**, 047203 (2019).

[19] M. K. Crawford, M. A. Subramanian, R. L. Harlow, J. A. Fernandez-Baca, Z. R. Wang, and D. C. Johnston, Phys. Rev. B **49**, 9198 (1994).

[20] Review articles include: J. G. Rau, E. K.-H. Lee, and H.-Y. Kee, Annu. Rev. Condens. Matter Phys. **7**, 195 (2016); J. Bertinshaw, Y. K. Kim, G. Khaliullin, and B. J. Kim, *ibid.* **10**, 315 (2019).

[21] G. Jackeli and G. Khaliullin, Phys. Rev. Lett. **102**, 017205 (2009).

[22] Y. Gao, Y. Gao, T. Zhou, H. Huang, and Q. H. Wang, Sci. Rep. **5**, 9251 (2015).

[23] We use the BNS setting of magnetic space groups; see Bilbao Crystallographic Server, http://www.cryst.ehu.es.

[24] D. Meyers, Y. Cao, G. Fabbris, N. J. Robinson, L. Hao, C. Frederick, N. Traynor, J. Yang, J. Lin, M. H. Upton, D. Casa, J. W. Kim, T. Gog, E. Karapetrova, Y. Choi, D. Haskel, P. J. Ryan, L. Horak, X. Liu, J. Liu, and M. P. M. Dean, Sci. Rep. **9**, 4263 (2019).

[25] K. Kobayashi, T. Nagao, and M. Ito, Acta Crystallogr., Sect. A **67**, 473 (2011).

[26] M. Fiebig, J. Phys. D: Appl. Phys. **38**, R123 (2005).

[27] M.-T. Suzuki, H. Ikeda, and P. M. Oppeneer, J. Phys. Soc. Jpn. **87**, 041008 (2018).

[28] F. Thöle and N. A. Spaldin, Phil. Trans. R. Soc. A **376**, 20170450 (2018).

[29] Y. Joly, http://www.neel.cnrs.fr./fdmnes.

[30] F. Cricchio, F. Bultmark, O. Grånäs, and L. Nordström, Phys. Rev. Lett. **103**, 107202 (2009).

[31] L. C. Chapon and S. W. Lovesey, J. Phys.: Condens. Matter **23**, 252201 (2011).

[32] F. Ye, S. Chi, B. C. Chakoumakos, J. A. Fernandez-Baca, T. Qi, and G. Cao, Phys. Rev. B **87**, 140406(R) (2013).

[33] B. J. Kim, H. Ohsumi, T. Komesu, S. Sakai, T. Morita, H. Takagi, and T. Arima, Science **323**, 1329 (2009).